Progress In Electromagnetics Research M, Vol. 69, 115–125, 2018

Design of a Compact CP Antenna with Enhanced Bandwidth Using a Novel Hexagonal Ring Based Reactive Impedance Substrate

Gopinath Samanta* **and Sekhar R. Bhadra Chaudhuri**

Abstract—A novel hexagonal ring-based reactive impedance surface (RIS) has been proposed and comprehensively employed as a ground plane of a circular polarized patch antenna (CPPA) for enhancing impedance bandwidth (IBW) and axial ratio bandwidth (ARBW), simultaneously. Furthermore, a simple analytical model analysis has been developed to estimate the resonance frequency and to predict the surface characteristics of the RIS structure. Two slits over the patch render the antenna to radiate circular polarized (CP) wave. The RIS has improved the CP antenna performance in terms of compactness, improved gain and increased efficiency. The proposed loaded structure has been numerically and experimentally studied with a layout of $40 \times 40 \times 3.2\,\text{mm}^3$ at 3.7 GHz. The measured results indicate that the prototype antenna has produced a relatively wider IBW and ARBW of 9.32% and 2.1%, respectively with peak gain about 2.98 dBiC. Both gain and efficiency of the loaded structure have been improved owing to the low conductive loss of the ring-shaped RIS. The proposed CP antenna might be suitable for radar application used in S-band.

1. INTRODUCTION

In recent years, small circular polarized antennas have intrigued a great impetus and been applied to numerous wireless communication systems due to their advantages such as light weight, easy fabrication and more significantly the independency of polarization orientation between transmitter and receiver [1, 2]. Several techniques like slit/slot loading over patch [3, 4], metamaterial inspired transmission line approach [2, 5] have been utilized to design small CP antenna. Unfortunately, these antennas provide low axial ratio bandwidth (AR < 3 dB) of less than 1%. Several techniques [6–8] were employed to solve this issue. However, the improvement in axial ratio bandwidth as well as impedance bandwidth was obtained at the increase of either lateral size [6] or vertical size [7, 8]. Nowadays, electromagnetic metamaterial [9, 10] and metasurface [11–18] have been intensely studied to counter the above two issues, i.e., miniaturization and bandwidth enhancement of CP antenna. In spite of the improvement in bandwidth both radiation efficiency and gain of the antenna are degraded in [9] while use of complementary split ring resonator (CSRR) structure has produced narrow return loss and axial ratio bandwidth in [10].

Reactive impedance surface (RIS), as a significant part of metasurface, has been widely used to reduce the size and improve the performance of linear polarized patch antenna [11]. Most recently, circular RIS and annular ring RIS have been applied to miniaturize the size and improve the performance of patch antenna [12, 13]. Moreover, RIS structure is not only employed to improve the performance of linear polarized antenna [11–13] but has also widely utilized to design miniaturized circular polarized antenna [14–19]. A wideband CP antenna has been realized in [14] using rotated square shaped patch based RIS with high permittivity material. Nevertheless, the structure lacks in compactness and low profile issue. In [15, 16], combination of square RIS and meta-resonators has been employed to design a

Received 10 April 2018, Accepted 29 May 2018, Scheduled 13 June 2018

* Corresponding author: Gopinath Samanta (gopi_samanta@yahoo.co.in).

The authors are with the Department of Electronics and Telecommunication Engineering, Indian Institute of Engineering Science and Technology, Shibpur Howrah, West Bengal, India.

compact CP antenna. However, structures in [15–17] have produced limited bandwidth and radiation efficiency. The problem featured in [8] in terms of compactness can be alleviated by introducing square RIS below the slotted patch antenna [17]. Compared to square patch RIS, Jerusalem cross RIS provides more gain and better impedance matching for the CP antenna [18]. Recently, a CP antenna has been miniaturized with high gain but low impedance bandwidth using fractal-based reactive impedance substrate [19].

Generally, the surface characteristic of RIS based configurations [14–19] is controlled by gap capacitance and shunted inductance which depends on uniform gap between adjacent patches and metal-backed substrate, respectively. There might be a scope to vary the edge capacitance by introducing nonuniform gap between two adjacent patches. Such implication of edge capacitance can be achieved by using hexagonal ring patches where adjacent elements have inherent nonuniform gap in one direction. Therefore, the use of hexagonal ring based RIS is capable of providing sufficient surface characteristics by only altering arm length or gap distance.

In this regard, a novel reactive impedance surface based on hexagonal ring structure is designed and analyzed. An analytical approach along with simulation has been presented to describe the reflection phase characteristics of the RIS. The hexagonal ring element has a lower level of metallization than square and circular elements [11–15] and contributes to lower resistive losses [18]. In addition to low losses, hexagonal ring RIS has also produced lower reactive surface impedance than square based RIS. Therefore, the proposed reactive surface becomes suitable to be employed as a ground plane of a CP antenna that has low input impedance. A probe fed hexagonal patch antenna is adopted for CP radiation by cutting two slits on the two opposite vertex of the radiating patch. The RIS is used in the inductive region for decreasing the resonance frequency and improving the antenna performance. Here, we have shown that the CP antenna has been miniaturized with significant improvement in both impedance bandwidth and axial ratio bandwidth by the ring based RIS configurations. The prototype antenna is capable to be used for S-band wireless applications.

The organization of the paper is as follows. hexagonal ring based RIS is discussed in Section 2. In Section 3 improvement of radiation performance of the CP antenna over the RIS is studied. Measured results of the fabricated prototype are discussed in the following section. A brief conclusion is drawn in Section 5.

2. DESIGN AND ANALYSIS OF HEXAGONAL RING BASED RIS

The reflection phase characteristics of the proposed RIS are realized by simulating the unit cell configuration shown in Figure 1. The unit cell is composed of a 2×2 array of hexagonal ring elements

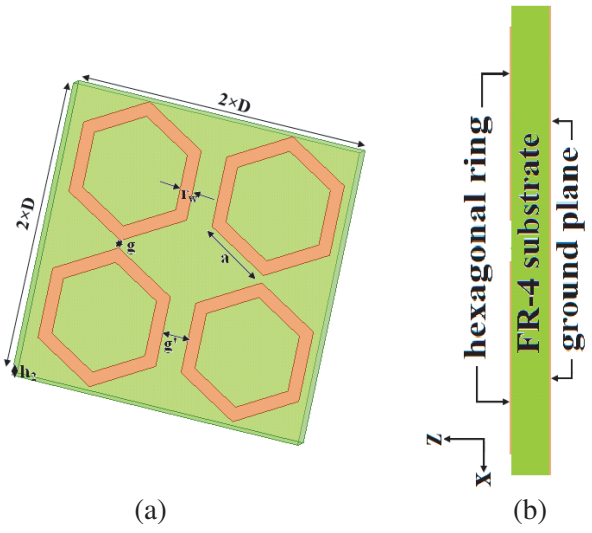

Figure 1. Unit cell configuration of hexagonal ring based RIS, (a) perspective view, (b) side view.

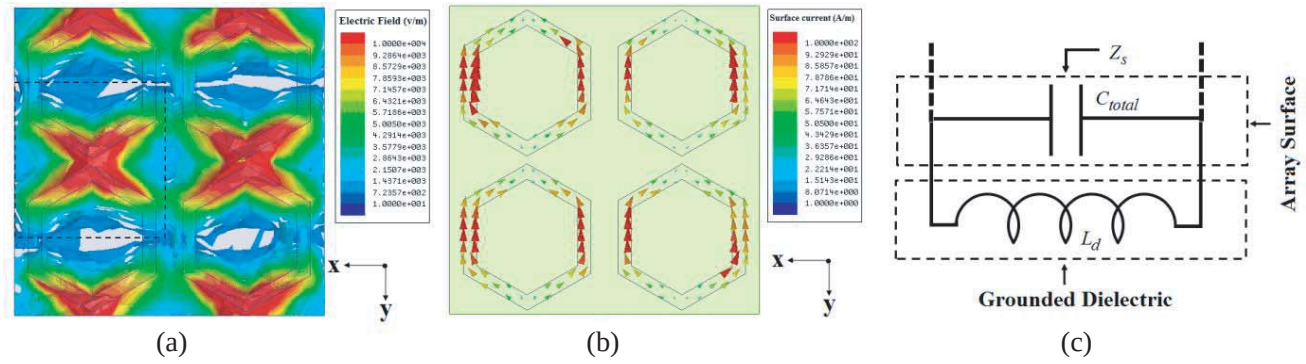

Figure 2. Distribution of (a) electric field, (b) electric current over the RIS elements, (c) analytical model.

which are printed over a metal backed FR-4 epoxy substrate. The substrate is characterized by dielectric constant of $\varepsilon_r = 4.4$ and loss tangent of $\tan\delta = 0.02$. To find the reflection phase and surface impedance characteristics the unit cell is simulated with the master slave boundary condition and floquet port excitation method using HFSS v.15. The unit cell structure resonates at 5.92 GHz and exhibits pure inductive behavior below the resonance frequency. Dimensions of unit cell structure are likewise; length of hexagonal arm $a = 4.75\,\text{mm}$, gap $g = 0.5\,\text{mm}$, ring width $r_w = 1\,\text{mm}$, periodicity $D = 10\,\text{mm}$, substrate height $h = 1.6\,\text{mm}$. Analytical model and the comparison between numerical and analytical responses have been elaborated in Subsections 2.1 and 2.2, respectively.

2.1. Analytical Model

An analytical approach has been presented to get an insight on reflection phase characteristics of the RIS for normal incidence of electromagnetic wave. In order to determine the equivalent circuit model, simulated electric field distribution and surface current distribution over the RIS are examined in Figure 2. It is apparent for Figure 2(a) that most of the field is concentrated between two adjacent ring-elements in the y-direction. This strong electric field between two adjacent V-Λ sections of hexagonal arms represents strong charge concentration that can be modeled by equivalent capacitive lumped component (C). In Figure 2(b), current distributions over the patch elements depict that maximum currents flowing in parallel two arms of the ring are in the same direction. These unidirectional current produces reverse magnetic fields which are mutually canceled out and do not contribute any inductance to the surface. Since the thickness of the substrate is smaller than quarter wavelength at the designed frequency, the PEC-backed substrate can be modeled by lumped inductor (L). Therefore, hexagonal ring RIS structure has been modeled by shunted combination of L and C parameter [15, 16].

To estimate the capacitance of the array surface, an assessment of average gap is required as the gap between two adjacent rings along y-direction is not uniform. The average gap can be determined by considering the maximum electric field region between adjacent ring elements. The clear view of maximum electric field region is shown in Figure 3(a) and marked by $AEBCB'E'A'D$ section. The average gap can be evaluated by integrating the whole region bounded by CD-DA-AE-EB-BC. However, here we consider only one half (OE-EB-BC-CO) of the full region, as rest of the region is just replica of the concerned region. The interested region is also marked by the blue line in Figure 3(a). The coordinate of vertices of the OEBC region is

$$O\,(0,0)\,,\ E\,(-x_0,0)\,,\ B=\left(-\frac{\sqrt{3}a}{2},-\frac{a+g}{2}\right),\ C\left(0,-\frac{g}{2}\right)$$

Area of the region bounded by the line BC and X-axis is

$$A_1=\int\limits_{x=-\frac{\sqrt{3}a}{2}}^{x=0}\left(\frac{x}{\sqrt{3}}-\frac{g}{2}\right)dx \tag{1}$$

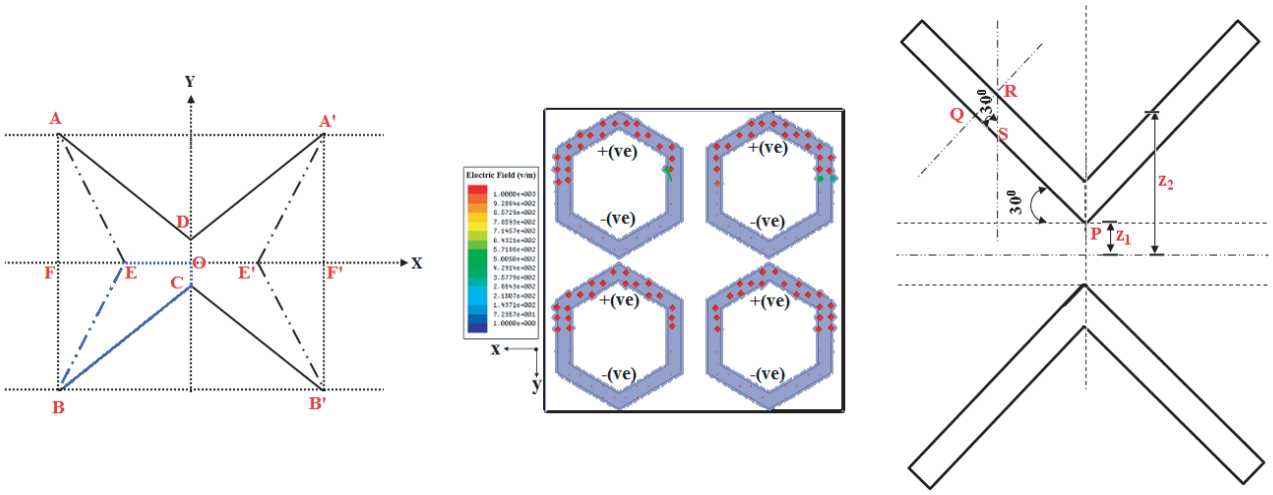

(a) (b) (c)

Figure 3. (a) Approximated graphical area of maximum field region between two hexagonal-ring elements, (b) positive and negative charge distribution over the ring arms, (c) effective ring width (RS) to determine C_0.

Area of the region bounded by the BE line and Y-axis is

$$A_2 = \int_{y=-\frac{a+g}{2}}^{y=0} \left[x_0 + \left(\frac{2}{a+g} \right) \left(-x_0 + \frac{\sqrt{3}a}{2} \right) y \right] dy \tag{2}$$

Now, average gap (g_{avg}) between two adjacent ring elements is

$$g_{avg} = \frac{2}{x_0} \left(A_1 + A_2 \right); \; x_0 = \frac{\sqrt{3}a}{2} n \tag{3}$$

Here, $n(< 1)$ is the fraction and is approximated by considering the maximum field region spreads along the horizontal axis. By considering $n = 0.8$, the average gap is calculated as 3.42 mm. Using this average gap, the gap capacitance (C_{total}) between two adjacent rings can be estimated by determining capacitance per unit length C_0. It is noted from Figure 3(c) that ring width (r_w) is modified to (r_{w1}) for determining C_0. In Figure 3(c) the variables are indicated as follows

$$\begin{aligned} &QR = r_w, \; RS = r_{w1}, \; r_{w1} = \sqrt{1 + \left(\frac{r_w}{\sqrt{3}} \right)^2}, \; Z_1 = \frac{g_{avg}}{2}, \; Z_2 = Z_1 + r_{w1} \\ &C_0 = \varepsilon \frac{K\left(p_2\right)}{K\left(p_1\right)}; \; p_1 = \frac{Z_2 - Z_1}{Z_2}, \; p_2 = \sqrt{1 - p_1^2}, \; Z_2 > Z_1 \end{aligned} \tag{4}$$

$K(p)$ is the complete elliptical integral defined as in [11].

$$K(p) = \int_0^{\frac{\pi}{2}} \frac{d\theta}{\sqrt{1 - p^2 \sin^2 \theta}} = \frac{\pi}{2} \left(1 + \frac{1^2}{2^2} p^2 + \frac{1^2}{2^2} \cdot \frac{3^2}{4^2} p^4 + \frac{1^2}{2^2} \cdot \frac{3^2}{4^2} \cdot \frac{5^2}{6^2} p^6 + \ldots \right), \; p < 1 \tag{5}$$

Using Equations (4)–(5) and above mentioned data C_0 is found to be 25 pF/m. Total effective length of the conductor $\tilde{a}$ is the summation of arm length of two inclined arms and half of each straight arm. The reason behind the extension of effective conductor length is easily understood from charge distribution plot depicted in Figure 3(b).

Thus, Total capacitance is computed as,

$$C_{\text{total}} = \tilde{a}C_0 \tag{6}$$

The inductance provided by the metal-backed substrate is expressed as in [13].

$$L_d = \mu_0\mu_r h \tag{7}$$

Now, the unit cell resonance frequency of the unit cell is calculated by the following equation.

$$f = \frac{1}{2\pi\sqrt{L_d C_{\text{total}}}} \tag{8}$$

2.2. Analysis of Unit Cell Response

Reflection phase and surface impedance characteristics of the proposed reactive impedance substrate are shown in Figures 4(a) and 4(b), respectively. The simulated structure resonates at 5.92 GHz and provides pure reactive surface impedance below the resonance. The analytical model provides value of $C_{\text{total}} = 0.36$ pF and $L_d = 2$ nH. Thus the model determines the null phase frequency at 5.96 GHz. Also, surface impedance characteristic of the model is closely matched with the simulation approach particularly below the unit cell resonance. It is expected that such hexagonal RIS while operating in inductive region would produce desired response after embedding it below a radiator. Generally two main properties of reactive impedance surface are utilized to achieve the desired performance. These include: 1) Minimization of mutual coupling between antenna and its image due to spatial distribution of image current; 2) Compensation of stored near field electric or magnetic energy within the two substrates.

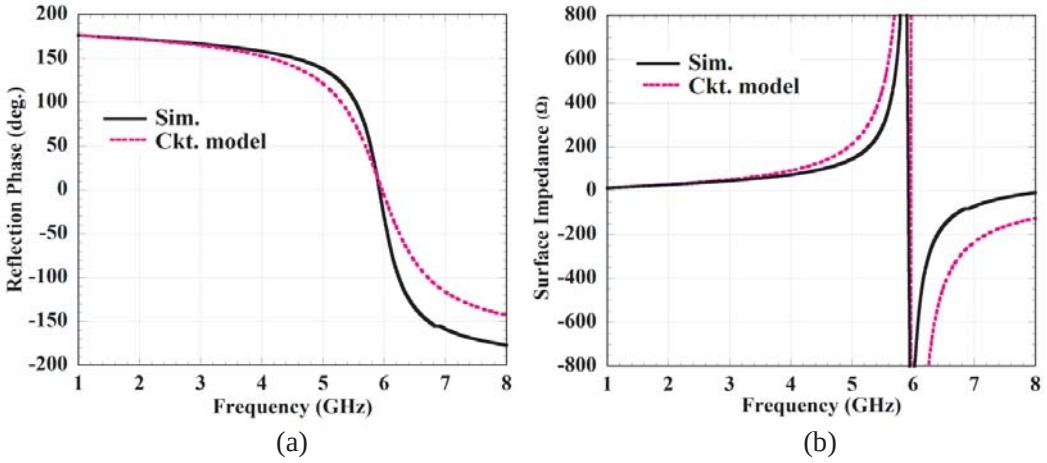

Figure 4. Unit cell characteristics for both approaches, (a) reflection phase, (b) surface impedance.

3. HEXAGONAL CIRCULAR POLARIZED ANTENNA OVER THE RIS

The reactive impedance surface realized in the previous section is employed here to miniaturize a CP patch antenna along with the enhanced impedance and axial ratio bandwidth. Initially, a simple hexagonal CP patch antenna with dimension of 20 mm × 17.3 mm is designed over an FR-4 substrate by cutting two slits at the two opposite vertices of the hexagonal patch. Two narrow slits provide two orthogonal modes that help to generate CP wave while appropriate feed location provides sufficient impedance matching. Thereafter, the hexagonal-ring RIS is used as antenna ground plane to enhance the image cancelation between radiator and ground plane.

To reduce the size and improve the CP performance, the simple antenna is placed over the RIS as depicted in Figure 5. Dimensions of the loaded structure are summarized in Table 1. The feed location of the loaded antenna is retained similar to the reference antenna while slit length (S_l) is slightly

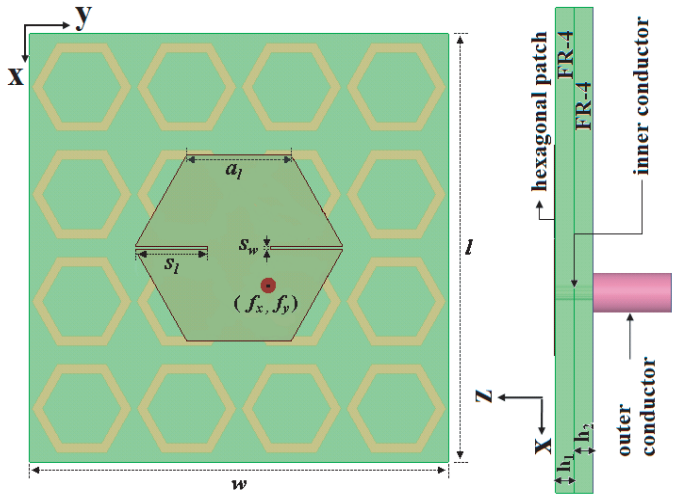

(a) (b)

Figure 5. RIS loaded CP antenna, (a) top view, (b) side view.

Table 1. Dimension of the RIS loaded structures (all units are in mm).

W	**L**	S_l	S_w	a_l	h_1	h_2	f_x	f_y
40	40	7	0.3	10	1.6	1.6	3.5	2.8

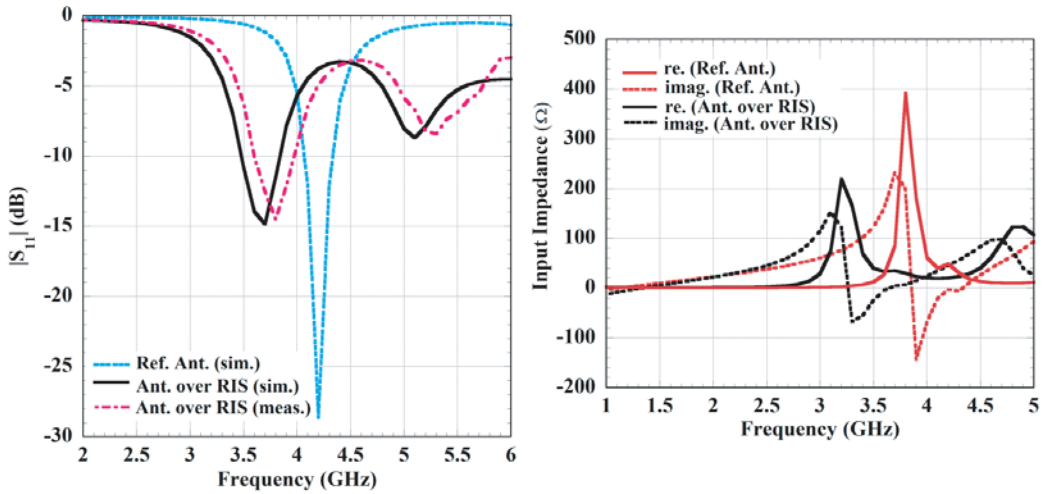

(a) (b)

Figure 6. (a) Return loss characteristics and (b) input impedance characteristics of reference and loaded antenna.

modified to excite two orthogonal modes for CP wave generation. The simple antenna resonates at 4.2 GHz with an impedance bandwidth of 6.33% and CP bandwidth of 0.59%. After the employment of RIS, the resonance frequency is shifted down to 3.7 GHz as observed from Figure 6(a), while impedance bandwidth and axial ratio bandwidth are calculated at 9.89% and 2.3%, respectively. A comparison of circular polarized performances between reference and RIS loaded antenna is highlighted in Table 2. Input impedance characteristics of reference as well as loaded antenna are plotted in Figure 6(b).

Table 2. Resonance and radiation performance of different antenna configurations.

Ant. type	Res. freq. (GHz)	Matching (dB)	IBW (%)	ARBW (%)	Peak Gain (dBiC)	Efficiency (%)	FBR (dB)	Co-pol and cross-pol isolation (dB)
Ref. Ant.	4.2	−28.6	6.33	0.59	3.19	59.44	18.86	18
RIS loaded Ant.	3.7	−14.86	9.89	2.3	3.24	75.62	23.06	22

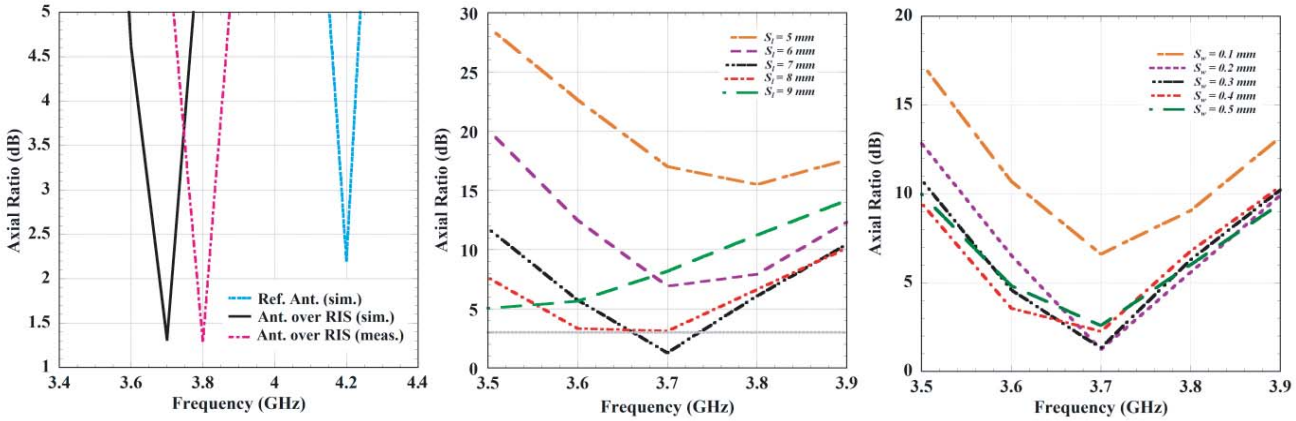

Figure 7. (a) Axial ratio characteristics of loaded and unloaded antenna; axial ratio characteristics of RIS loaded antenna with the variation of (b) slit length and (c) slit width.

The principle behind the antenna miniaturization and bandwidth improvement using hexagonal RIS is explained by the compensation of near field energy stored within the two substrates. The reference antenna provides capacitive impedance below 4.2 GHz while in the same frequency range RIS produces inductive behavior. As a consequence, energy stored in the antenna substrate and RIS substrate are canceled out below the patch resonance. Therefore, energy storage within the patch substrates gets reduced that signifies the degradation in antenna quality factor which in turn suggests the enhancement of impedance bandwidth. Axial ratio characteristics of both antenna configurations are depicted in Figure 7(a). A parametric study is shown in Figures 7(b)–(c) to find the suitable dimension of length and width of the rectangular slit. It is seen that reduction of slit length deteriorates the CP performance while variation of slit width has relatively less effect on the antenna axial ratio. From Figure 7(c), it is found that maximum CP bandwidth of the RIS loaded structure is obtained for $S_W = 0.3$ mm and $S_l = 7$ mm.

The enhancement in ARBW can be explained with the help of Figure 8 which depicts the phase difference and amplitude ratio of two orthogonal field components. Location of the feed point plays an important role to determine impedance matching as well as types of polarization. Left-handed circular polarized (LHCP) wave is generated by exciting the patch at (f_x, f_y) location, while RHCP wave would be generated by placing the feed point at $(f_x, -f_y)$ position. The position of feed point is determined with respect to centre of the hexagonal patch. Also, the generation of two circular polarized waves can be explained by the phase difference between two longitudinal field components (E_y and E_x) and the amplitude ratio between E_y and E_x at the antenna resonance frequency and is exhibited in Figure 9. It is found that for RIS loaded antenna, the electric field ratio (FR) and phase difference (δ) are 0.99 and 82°, respectively for feed location of (f_x, f_y), while feed position of $(f_x, -f_y)$ produces FR = 0.9 and $\delta = -99°$ at 3.7 GHz. Positive value of δ indicates LHCP radiation whereas negative δ signifies RHCP wave.

Radiation patterns of the loaded antenna are depicted in Figure 9 at both E-plane and H-plane.

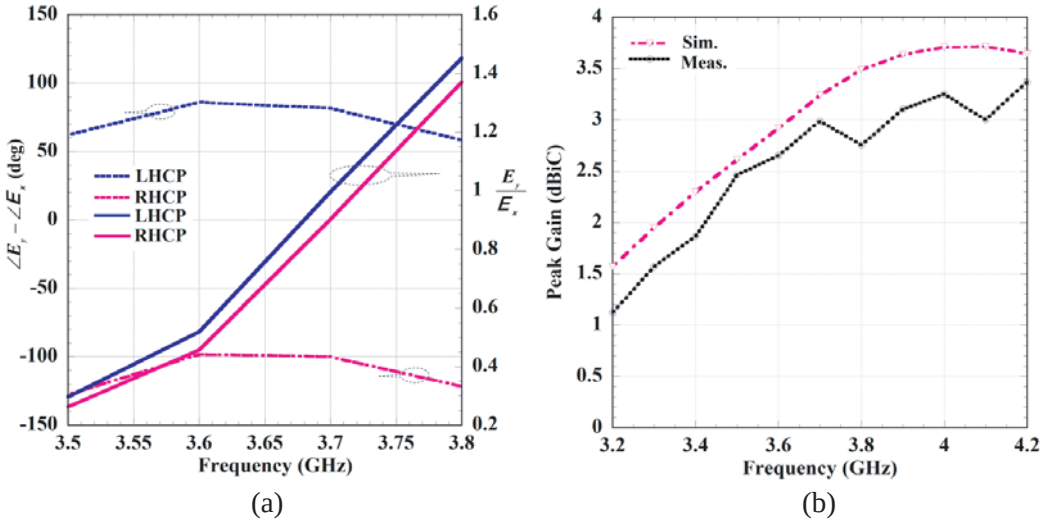

Figure 8. (a) Phase difference and magnitude ratio between two orthogonal fields of RIS loaded antenna, (b) peak gain versus frequency plot of the RIS loaded antenna.

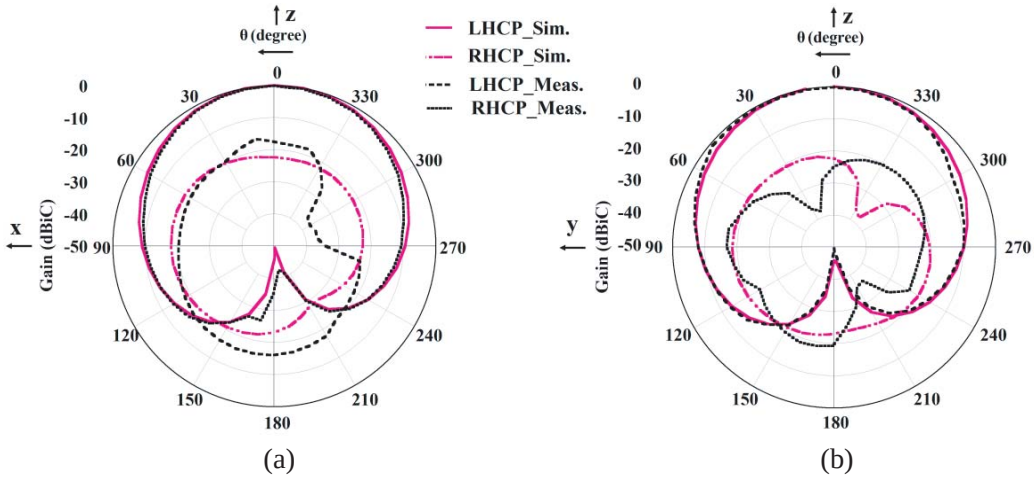

Figure 9. LHCP radiation pattern of RIS loaded antenna in (a) E-plane, (b) H-plane.

Simulated peak gain is noted as 3.24 dBic which is slightly improved compared to the reference CP antenna. Also, the gain versus frequency plot is included in Figure 8(b). The efficiency of the loaded antenna is observed to be increased to 75.62% from an efficiency of 59.44% for the unloaded antenna. With the introduction of RIS below the patch, front-to-back ratio of the prototype antenna has also been improved by 4 dB compared with the reference structure. The 3 dB axial ratio beamwidth is more than 122° in the global bandwidth region.

To get a straight forward realization of the radiated CP wave by the RIS loaded antenna, a time domain analysis of the electric field at 3.7 GHz is illustrated in Figure 10. It is apparent that initially the field was concentrated at Y direction in X-Y plane, and with the progression of time the electric field is rotated in clockwise direction that represents LHCP nature of the radiated wave.

4. FABRICATION AND EXPERIMENTAL RESULT

Finally, the well designed doubled layer structure shown in Figure 5 is fabricated and assembled for the measurement purpose. Photographs of the fabricated prototype are displayed in Figure 11. The two

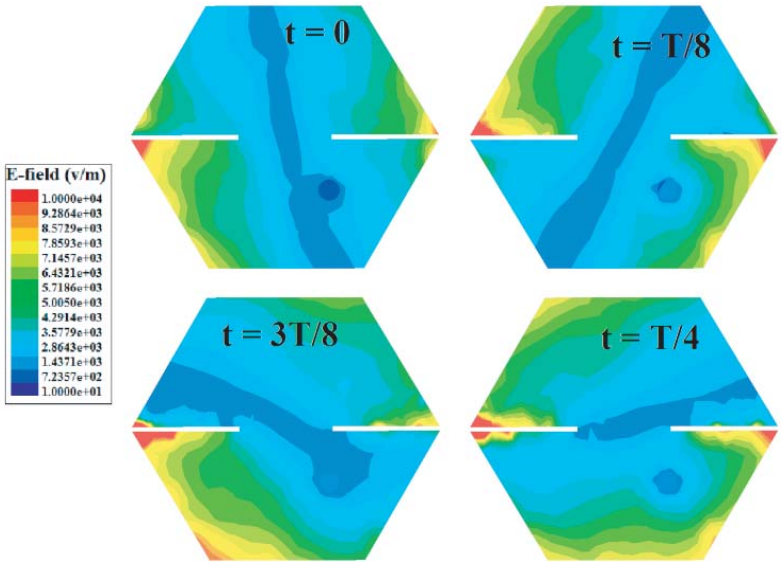

Figure 10. Electric field distribution on the patch antenna in time domain at 3.7 GHz.

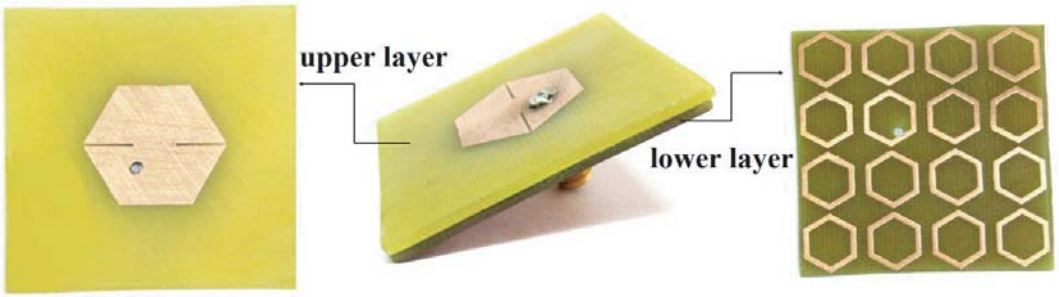

Figure 11. Fabricated prototype antenna; top view of (a) radiating patch, (b) RIS structure, (c) perspective view of RIS loaded antenna.

substrates with equal footprints are aligned properly and then bonded tightly by an adhesive. To avoid any contact with the inner conductor a small segment is etched from the nearest hexagonal ring patch. An SMA connector having an inner conductor radius of 0.7 mm with a height of ($h_1 + h_2 = 3.2$ mm) is inserted within the structure through the feed-hole into the assembly. Return loss characteristic of the proposed structure is measured using Anritsu MS2025B vector network analyser while CP radiation pattern is measured using far field measurement system in an anechoic chamber.

Figure 6(a) and Figure 7 compare the simulated and measured return loss and axial ratio characteristics, respectively. A frequency shifting in measured resonance is noted which may happen due to the inherent tolerances in fabrication process. The impedance bandwidth and axial ratio bandwidth for the fabricated prototype are measured at 9.32% and 2.1%, respectively. It is worth to note that axial ratio bandwidth lies completely within 10 dB impedance bandwidth in the measured state.

To study the radiation performance of the fabricated antenna, co-pol (LHCP) and cross-pol (RHCP) are measured at both E plane and H plane at the resonance. It is found from Figure 9 that measured radiation pattern is well matched with the simulated result at both polarization planes. The fabricated antenna provides maximum measured LHCP gain at the boresight direction at 2.98 dBiC. The radiation efficiency of the antenna is measured at 70.5%. The proposed CP antenna is suitable for wireless application due to its comparable gain, good axial ratio bandwidth and acceptable radiation efficiency.

Table 3. Comparison of CP performances of the proposed antenna with some recent RIS loaded CP antenna.

Lit.	RIS Patch	Res. Freq. (GHz)	IBW (%)	ARBW (%)	Peak Gain (dBic)	Efficiency (%)	Co-cross Isolation (dB)	RIS Thickness
[15]	Square	2.8	5.03	1.6	–	80	–	$0.025\lambda_0$
[16]	Square	2.86	1.75	1.05	4.15	67.6	19.4	$0.01\lambda_0$
[17]	Square	2.5	5.2	1.6	3.41	–	28	$0.026\lambda_0$
[18]	J-cross	1.18	1.44	2.21	2.88	–	24	$0.013\lambda_0$
[19]	Fractal	3.5	3.77	1.58	6.3	91.5	18.5	$0.017\lambda_0$
Our Work	Hexa-ring	3.7	9.89	2.3	3.24	75.62	22.4	$0.019\lambda_0$

Table 3 compares the performance of proposed prototype with some recent RIS-loaded CP antennas. It is observed that our RIS structure provides maximum bandwidth in return loss and axial ratio compared to [15–19]. Gain of the proposed antenna is comparable to [17, 18] while co-cross pol isolation is slightly better than [16, 19]. The RIS thickness of the proposed structure is also comparable to [15, 17, 18]. Lower RIS profile was achieved in [16, 18] but at the cost of degraded bandwidth. The profile of our prototype antenna is slightly larger by $0.01\lambda_0$ than [15–19], but the proposed structure is cost effective, light weight and low-loss owing to the use of ring-shaped RIS structure and inexpensive substrate.

5. CONCLUSION

In this paper, a unit cell structure based on hexagonal-ring element has been adopted to design a reactive impedance surface substrate. Thereafter, CP performances of a patch antenna have been improved by loading the RIS substrate below the antenna substrate. An analytical approach based on electric field and surface current distribution has been established to investigate the unit cell characteristics. Furthermore, the simulated responses are compared with the analytical results. A parametric analysis has been conducted to find the appropriate length and width of the slit. The RIS substrate improves the antenna performance by 1.5 times in CP bandwidth and about four times in return loss bandwidth. In addition to the bandwidth enhancement and miniaturization, the gain and efficiency are also improved by the reactive substrate. The resonance of the fabricated prototype is measured at 3.8 GHz with an ARBW of 2.1% and peak gain of 2.98 dBic. Based on previous studies it can be concluded that exploitation of the proposed RIS is superior to conventional square RIS in perspective of improvement in bandwidth and radiation performances. Numerical and experimental results suggest that the proposed antenna, possessing a maximum dimension of $0.246\lambda_0 \times 0.213\lambda_0 \times 0.039\lambda_0$ at 3.7 GHz, exhibits acceptable gain, efficiency and improved bandwidth, predicting some promising applications in S-band communication.

ACKNOWLEDGMENT

For research support, G. Samanta acknowledges Indian Institute of Engineering Science and Technology Shibpur.

REFERENCES

1. Li, R., J. Laskar, and M. M. Tentzeris, "Broadband circularly polarized rectangular loop antenna with impedance matching," *IEEE Microw. Wireless Compon. Lett.*, Vol. 16, No. 1, 52–54, Jan. 2006.
2. Park, B.-C. and J.-H. Lee, "Omnidirectional circularly polarized antenna utilizing zeroth-order resonance of epsilon negative transmission line," *IEEE Trans. Antennas Propag.*, Vol. 59, No. 7, 2717–2720, Jul. 2011.

3. Nasimuddin, Z. N. Chen, and X. Qing, "Slotted microstrip antennas for circular polarization with compact size," *IEEE Antennas and Propag. Mag.*, Vol. 55, No. 2, 124–137, Apr. 2013.
4. Yang, K.-P. and K.-L. Wong, "Dual-band circularly-polarized square microstrip antenna," *IEEE Trans. Antennas Propag.*, Vol. 49, No. 3, 377–382, Mar. 2001.
5. Ko, S.-T., B.-C. Park, and J.-H. Lee, "Dual-band circularly polarized patch antenna with first positive and negative modes," *IEEE Antennas Wireless Propag. Lett.*, Vol. 12, 1165–1168, Sep. 2013.
6. Yi, Y., L. J. Ying, W. Kun, X. Rui, and Y. G. Wei, "Circularly polarised cut ring microstrip antenna," *Electronics Lett.*, Vol. 51, No. 3, 199–200, Feb. 2015.
7. Tong, K.-F. and T.-P. Wong, "Circularly polarized U-slot antenna," *IEEE Trans. Antennas Propag.*, Vol. 55, No. 8, 2382–2385, Aug. 2007.
8. Khidre, A., K. F. Lee, F. Yang, and A. Elsherbeni, "Wideband circularly polarized E-shaped patch antenna for wireless applications," *IEEE Antennas Propag. Mag.*, Vol. 52, No. 5, 219–229, Oct. 2010.
9. Park, B.-C. and J.-H. Lee, "Dual-band omnidirectional circularly polarized antenna using zeroth- and first-order modes," *IEEE Antennas Wireless Propag. Lett.*, Vol. 11, 407–410, Apr. 2012.
10. Zhang, H., Y.-Q. Li, X. Chen, Y.-Q. Fu, and N.-C. Yuan, "Design of circular/dual-frequency linear polarization antennas based on the anisotropic complementary split ring resonator," *IEEE Trans. Antennas Propag.*, Vol. 57, No. 10, 3352–3355, Oct. 2009.
11. Mosallaei, H. and K. Sarabandi, "Antenna miniaturization and bandwidth enhancement using a reactive impedance substrate," *IEEE Trans. Antennas Propag.*, Vol. 52, No. 9, 2403–2414, Sep. 2004.
12. Samanta, G., D. Mitra, and S. R. B. Chaudhuri, "Miniaturization of a patch antenna using circular reactive impedance substrate," *Int. Journal of RF and Microwave Computer-Aided Engg.*, Vol. 27, No. 8, May 1–10, 2017.
13. Ghosh, A., T. Mandal, and S. Das, "Design and analysis of annular-ring based RIS its use in dual-band patch antenna miniaturization for wireless communication," *Journal of Electromagnetic Waves and Applications*, Vol. 31, No. 3, 335–349, Jan. 2017.
14. Bernard, L., G. Chertier, and R. Sauleau, "Wideband circularly polarized patch antennas on reactive impedance substrates," *IEEE Antennas Wireless Propag. Lett.*, Vol. 10, 1015–1018, Sep. 2011.
15. Dong, Y., H. Toyao, and T. Itoh, "Design and characterization of miniaturized patch antennas loaded with complementary split-ring resonators," *IEEE Trans. Antennas Propag.*, Vol. 60, No. 2, 772–785, Feb. 2012.
16. Xu, H.-X., G.-M. Wang, J.-G. Liang, M. Q. Qi, and X. Gao, "Compact circularly polarized antennas combining metasurfaces and strong space-filling meta-resonators," *IEEE Trans. Antennas Propag.*, Vol. 61, No. 7, 3442–3450, Jul. 2013.
17. Agarwal, K., Nasimuddin, and A. Alphones, "RIS based compact circularly polarized microstrip antennas," *IEEE Trans. Antennas Propag.*, Vol. 61, No. 2, 547–554, Feb. 2013.
18. Agarwal, K., Nasimuddin, and A. Alphones, "Triple-band compact circularly polarized stacked microstrip antenna over reactive impedance meta-surface for GPS applications," *IET Microw., Antennas, Propag.*, Vol. 8, No. 13, 1057–1065, Apr. 2014.
19. Cai, T., G.-M. Wang, X.-F. Zhang, and J.-P. Shi, "Low-profile compact circularly-polarized antenna based on fractal metasurface and fractal resonator," *IEEE Antennas Wireless Propag. Lett.*, Vol. 14, 1072–1076, Jan. 2015.